Research Square

Preprints are preliminary reports that have not undergone peer review.
They should not be considered conclusive, used to inform clinical practice,
or referenced by the media as validated information.

Gut Microbiota-Derived Indole-3-Acetic Acid Induces PCOS by Disrupting Granulosa Cell Function under Metabolic Stress

Yan Wang
Lanzhou University
Zhijian Luo
Lanzhou University
Ting Yang
Lanzhou University
Xiaorong Luo
Lanzhou University
Xuehong Zhang
zhangxueh@lzu.edu.cn
Lanzhou University

Research Article

Keywords: Polycystic ovary syndrome, Bacteroides fragilis, Indole-3-acetic acid, Aryl hydrocarbon receptor, Cell cycle

Posted Date: July 15th, 2026

DOI: https://doi.org/10.21203/rs.3.rs-9879889/v1

License: This work is licensed under a Creative Commons Attribution 4.0 International License.
Read Full License

Additional Declarations: No competing interests reported.

Version of Record: A version of this preprint was published at Journal of Ovarian Research on October 21st, 2026. See the published version at https://doi.org/10.1186/s13048-026-02306-4.

Abstract

Background

Polycystic ovary syndrome (PCOS) is a multifactorial reproductive and metabolic disorder, but the mechanisms linking metabolic stress to ovarian dysfunction remain incompletely understood. Gut microbiota-derived metabolites have emerged as important mediators of host metabolism; however, their contribution to PCOS pathogenesis, particularly within the ovarian microenvironment, remains poorly defined. This study aimed to identify microbiota-associated metabolic alterations in PCOS and determine their functional relevance under metabolically stressed conditions.

Results

Integrated clinical microbiota and metabolomic profiling revealed altered gut microbial composition and indole-related metabolic signatures in women with PCOS and overweight/obesity. Among the altered features, *Bacteroides fragilis* and indole-3-acetic acid (IAA) were selectively enriched and positively correlated. IAA was increased not only in fecal metabolic profiles but also in serum and follicular fluid, suggesting a link between gut-associated metabolic changes and the ovarian follicular microenvironment. Functional experiments showed that neither *B. fragilis* nor IAA alone was sufficient to induce PCOS-like phenotypes under basal conditions. In contrast, both *B. fragilis* and IAA promoted ovarian dysfunction, endocrine disturbance, and estrous cycle abnormalities under high-fat diet (HFD)-induced metabolic stress. At the cellular level, IAA suppressed granulosa cell proliferation by inhibiting G1/S cell-cycle progression and activating aryl hydrocarbon receptor (AHR) signaling. Pharmacological inhibition or knockdown of AHR partially reversed IAA-induced cell-cycle arrest. Moreover, lipotoxic stress enhanced IAA-induced AHR activation and cell-cycle inhibition, potentially through increased oxidative and endoplasmic reticulum stress.

Conclusions

These findings identify a context-dependent *B. fragilis*–IAA–AHR axis that links gut microbial metabolism to ovarian dysfunction under metabolic stress. The study provides mechanistic insight into the gut–ovary interaction in PCOS and suggests that microbiota-derived indole metabolites may contribute to disease progression in a metabolically permissive host environment.

Highlights

Gut microbiota-derived indole-3-acetic acid is selectively enriched in obese women with PCOS and is associated with *Bacteroides fragilis*.

IAA promotes PCOS-like phenotypes under high-fat diet conditions, indicating a context-dependent microbe-metabolite effect.

IAA suppresses granulosa cell proliferation via AHR-dependent inhibition of G1/S cell cycle progression, linking metabolic stress to ovarian dysfunction.

Introduction

Polycystic ovary syndrome (PCOS) is a common endocrine and metabolic disorder in women of reproductive age, affecting approximately 6–15% of the population[1–3]. Characterized by ovulatory dysfunction, hyperandrogenism, and polycystic ovarian morphology, PCOS is frequently accompanied by metabolic abnormalities such as insulin resistance, dyslipidemia, and obesity[2, 4, 5]. These manifestations indicate that PCOS is not only a reproductive disorder but also a complex metabolic syndrome with both local and systemic disturbances[6, 7].

Obesity, observed in 50–70% of PCOS patients, has been shown to exacerbate both the reproductive and metabolic features of the syndrome[8, 9]. Increased adiposity contributes to insulin resistance, promotes androgen overproduction, and disrupts the regulation of the hypothalamic-pituitary-ovarian axis[10, 11]. This is particularly evident in clinical settings, where obese PCOS patients tend to exhibit more severe hormonal imbalances compared to their lean counterparts[12–14]. The interaction between obesity and PCOS highlights obesity as a key modulator of the syndrome's severity and a critical factor influencing the progression of both metabolic and reproductive abnormalities[13, 15, 16].

Over the past decade, the gut microbiota has emerged as a key player in metabolic regulation, and its dysbiosis has been implicated in several metabolic disorders[17–19], including PCOS[20, 21]. Gut microbial composition influences host metabolism through pathways related to energy balance, immune modulation, and endocrine signaling[22, 23]. Recent studies have identified changes in gut microbiota composition in women with PCOS, with alterations in microbial diversity and abundance linked to insulin resistance, obesity, and hormonal imbalances[24–26]. Microbiota-derived metabolites, including short-chain fatty acids, bile acids, and indole derivatives, are thought to mediate the effects of microbiota alterations on host metabolic and immune systems[27–29].

Tryptophan metabolism has garnered particular attention in recent years as a potential link between gut microbiota and metabolic dysfunction. Gut microbes convert tryptophan into a range of bioactive metabolites, such as kynurenine and indole derivatives, which are involved in immune regulation, neuroendocrine signaling, and barrier function[30–32]. Disruptions in tryptophan metabolism are associated with various metabolic disturbances, including insulin resistance, obesity, and low-grade inflammation, all of which are relevant to the pathophysiology of PCOS.

In this study, we aimed to investigate the role of tryptophan metabolism in PCOS by comparing the gut microbiota composition and related metabolic features between women with PCOS and healthy controls. We specifically focused on indole derivatives, which are metabolites of tryptophan, and

examined their association with hormonal parameters in PCOS. We hypothesized that alterations in tryptophan metabolism, mediated by changes in gut microbiota, contribute to the metabolic and hormonal abnormalities seen in PCOS.

Methods

Clinical participant recruitment

Women of reproductive age with overweight/obesity, defined as a body mass index (BMI) ≥ 24 kg/m² according to the Chinese adult BMI classification, were recruited from Gansu Provincial Maternity and Child-care Hospital. Participants were assigned to the polycystic ovary syndrome (PCOS) group or the control group according to the Rotterdam diagnostic criteria. The control group comprised women undergoing assisted reproductive treatment for tubal factor infertility or male factor infertility, with regular menstrual cycles, no clinical or biochemical evidence of hyperandrogenism, and no polycystic ovarian morphology on ultrasound.

Written informed consent was obtained from all participants before enrollment. The study protocol was approved by the Ethics Committee of Gansu Provincial Maternity and Child-care Hospital (approval no. LDYYLL2024-257). Participants were excluded if they had any of the following conditions: endocrine disorders other than PCOS, including thyroid dysfunction or adrenal disease; recent use of antibiotics, oral contraceptives, or other medications known to interfere with endocrine function; severe cardiovascular disease, diabetes mellitus, or other chronic systemic diseases that could affect metabolic or reproductive status. All participants underwent detailed clinical assessment and physical examination at recruitment.

Measurement of indole-related metabolites in clinical samples

Peripheral blood samples were collected in the morning after an overnight fast. Serum was separated by centrifugation at 1,500 × g for 10 min at 4°C. Follicular fluid was collected during oocyte retrieval. Only macroscopically clear follicular fluid without visible blood contamination was used for subsequent analysis. Follicular fluid samples were centrifuged at 1,500 × g for 10 min at 4°C to remove cells and debris. Serum and follicular fluid supernatants were aliquoted immediately and stored at − 80°C until analysis. Repeated freeze-thaw cycles were avoided.

The concentrations of indole-3-acetic acid (IAA), indole-3-propionic acid (IPA), 5-hydroxytryptamine (5-HT), and melatonin (MT) in serum and follicular fluid were quantified using enzyme-linked immunosorbent assay (ELISA) kits according to the manufacturers' instructions. The following commercial kits were used: IAA ELISA kit (RUIXIN BIO, Cat. No. JRXW999086), IPA ELISA kit (ZCi BiO, Cat. No. ZC-53467), 5-HT ELISA kit (RUIXIN BIO, Cat. No. JRXW867956), and MT ELISA kit (RUIXIN BIO, Cat. No. JRXW999216). All samples were assayed in duplicate, and concentrations were calculated from standard curves generated in the same assay run.

Animals, housing conditions, and ethics statement

Six-week-old female C57BL/6J mice were purchased from GemPharmatech Co., Ltd. (Jiangsu, China). All mice were housed under specific pathogen-free (SPF) conditions at the Laboratory Animal Center of Lanzhou University, with an ambient temperature of 22 ± 2°C, relative humidity of 50%-60%, and a 12-h light/dark cycle. Mice had free access to food and water throughout the study. All animal procedures were conducted in accordance with institutional guidelines for laboratory animal care and use and were approved by the Ethics Committee of Gansu Provincial Maternity and Child-care Hospital/Lanzhou University under the same project approval number used for this study (LDYYLL2024-257).

Animal grouping and intervention protocol

After 1 week of acclimatization, mice were randomly assigned to the following experimental groups: control, high-fat diet (HFD), HFD plus *Bacteroides fragilis* intervention, and HFD plus indole-3-acetic acid (IAA) intervention. Mice in the control group were fed a standard chow diet, whereas mice in the HFD-related groups were fed a 60 kcal% fat HFD (XIETONG BIO, Cat. No. XTHF60). Dietary intervention and corresponding treatments were initiated simultaneously and continued for 12 weeks.

For bacterial intervention, *Bacteroides fragilis* was obtained from MINGZHOUBIO (Cat. No. B301873). The strain was cultured under anaerobic conditions and harvested during the logarithmic growth phase. Fresh bacterial suspensions were prepared before administration and delivered by oral gavage at approximately 5×10^8 colony-forming units (CFU) per mouse once daily for 12 weeks. Mice not receiving bacterial treatment were gavaged with an equal volume of vehicle.

For IAA intervention, IAA (MCE, Cat. No. HY-18569) was dissolved in sterile phosphate-buffered saline (PBS) and administered by intraperitoneal (i.p.) injection at 50 mg/kg body weight once daily for 12 weeks. Mice not receiving IAA treatment were injected with an equal volume of sterile PBS.

Estrous cycle monitoring

Estrous cyclicity was monitored during the late stage of the intervention period using vaginal cytology. Vaginal smears were collected at a fixed time each morning for 10 consecutive days. Smears were fixed in methanol, stained, and examined under a light microscope. Estrous cycle stages were classified as proestrus, estrus, metestrus, or diestrus according to the relative proportions of nucleated epithelial cells, cornified epithelial cells, and leukocytes.

Tissue collection and phenotypic analysis

At the end of the 12-week intervention, mice were fasted for 12 h. Mice were then deeply anesthetized with isoflurane inhalation (4% for induction and 1.5–2% for maintenance in oxygen). Adequate anesthesia was confirmed by the absence of the pedal withdrawal reflex. Blood samples were collected

via cardiac puncture or orbital sinus while mice remained under deep anesthesia. Following blood collection, mice were euthanized by carbon dioxide (CO_2) inhalation at a displacement rate of approximately 20% chamber volume per minute, in accordance with the AVMA Guidelines for the Euthanasia of Animals. Death was confirmed by cessation of respiration and heartbeat. Ovaries and inguinal white adipose tissue (iWAT) were then collected. Ovarian tissues were fixed in 4% paraformaldehyde, embedded in paraffin, sectioned at 5 μm, and stained with hematoxylin and eosin (H&E) to assess follicular development and ovarian morphology.

Inguinal white adipose tissue was carefully dissected and weighed to calculate the iWAT-to-body weight ratio. For lipid deposition and adipocyte morphology analysis, iWAT samples were embedded for frozen sectioning and subjected to Oil Red O staining.

Serum hormone and metabolite measurements

Blood samples were allowed to clot and then centrifuged at 1,500 × g for 10 min at 4°C to isolate serum. Serum samples were aliquoted and stored at − 80°C until analysis, and repeated freeze-thaw cycles were avoided.

Serum concentrations of testosterone (RUIXIN BIO, Cat. No. RXJW202530M), luteinizing hormone (LH; RUIXIN BIO, Cat. No. RXJW202015M), follicle-stimulating hormone (FSH; RUIXIN BIO, Cat. No. RXJW203000M), and estradiol (E2; RUIXIN BIO, Cat. No. RXJW203008M) were measured using enzyme-linked immunosorbent assay (ELISA) kits according to the manufacturers' instructions.

Serum levels of indole-related metabolites, including indole-3-acetic acid (IAA), indole-3-propionic acid (IPA), 5-hydroxytryptamine (5-HT), and melatonin (MT), were quantified using ELISA kits as described for the clinical samples. All assays were performed according to the corresponding kit protocols, with samples measured in duplicate whenever sufficient serum volume was available.

Cell culture and treatments

The human ovarian granulosa-like tumor cell line KGN was obtained from MINGZHOUBIO. Cells were cultured in Dulbecco's modified Eagle's medium/Ham's F-12 medium (DMEM/F12; Gibco, Cat. No. 11330032) supplemented with 10% fetal bovine serum (FBS; Gibco, Cat. No. 10099141C) and 1% penicillin-streptomycin. Cells were maintained at 37°C in a humidified incubator with 5% CO_2. Cells at approximately 70%-80% confluence were used for experiments.

Preparation of PA-BSA complex and establishment of the lipotoxicity model

Palmitic acid (PA; Sigma-Aldrich, Cat. No. P0500) was prepared as a fatty acid-free bovine serum albumin (BSA)-conjugated complex before cell treatment. Briefly, PA was dissolved in 0.1 M NaOH at

70°C to generate a 100 mM stock solution. The PA solution was then slowly added to prewarmed fatty acid-free BSA solution and incubated at 55°C with continuous agitation to allow conjugation. The final PA-BSA stock solution was prepared at 5 mM PA in 10% BSA, sterile-filtered, aliquoted, and stored at −20°C. Before use, the stock solution was warmed and diluted in complete culture medium to the indicated working concentration. Vehicle control medium contained the corresponding concentration of BSA.

To establish an in vitro lipotoxicity model, KGN cells were treated with 200 μM PA-BSA for 48 h. For IAA intervention, cells were treated with 10 μM indole-3-acetic acid (IAA; Sigma-Aldrich, Cat. No. I3750). The experimental groups included control, PA, IAA, and PA + IAA groups. In the combined treatment group, cells were exposed to PA-BSA and IAA under the same culture conditions, with BSA-treated cells used as the vehicle control.

AHR inhibition and lentiviral knockdown

To examine whether aryl hydrocarbon receptor (AHR) signaling was required for the effects of IAA, AHR activity was blocked using the selective AHR antagonist CH-223191 or genetically suppressed using lentivirus-mediated knockdown. For pharmacological inhibition, KGN cells were pretreated with CH-223191 (MCE, Cat. No. HY-12684) at 10 μM for 1 h before IAA treatment, and CH-223191 was maintained in the culture medium during subsequent treatment.

For AHR knockdown, lentiviral particles carrying short hairpin RNA targeting AHR (shAHR) or a non-targeting control sequence (shNC) were obtained from Hanbio Biotechnology. KGN cells were seeded to reach 40%-50% confluence at the time of infection and transduced with lentivirus at a multiplicity of infection (MOI) of 30 in the presence of 8 μg/mL polybrene. After 24 h, the viral medium was replaced with fresh complete medium. At 48 h after infection, cells were selected with puromycin at 2 μg/mL for 3–5 days to establish AHR-knockdown cells. Knockdown efficiency was confirmed by quantitative real-time polymerase chain reaction (qPCR) and Western blotting before functional assays.

After AHR inhibition or knockdown, cells were subjected to the indicated PA and/or IAA treatments and then harvested for cell-cycle analysis, Western blotting, qPCR, or other downstream assays to determine whether suppression of AHR signaling attenuated the IAA-mediated effects.

Cell viability assay

Cell viability was measured using the Cell Counting Kit-8 (CCK-8) assay. KGN cells were seeded into 96-well plates and allowed to adhere overnight. Cells were then treated with increasing concentrations of IAA, including 10, 20, 40, 80, 160, 320, and 640 μM. After treatment, CCK-8 reagent (Dojindo, Cat. No. CK04) was added to each well, and cells were incubated at 37°C for 1–2 h protected from light. Absorbance was measured at 450 nm using a microplate reader. Cell viability was calculated relative to the control group and expressed as a percentage.

CFSE-based proliferation assay

Cell proliferation was assessed using carboxyfluorescein succinimidyl ester (CFSE) dilution. KGN cells were detached with trypsin and resuspended in prewarmed phosphate-buffered saline (PBS) or serum-free medium. Cells were labeled using the CellTrace™ CFSE Cell Proliferation Kit (Invitrogen, Cat. No. C34554) according to the manufacturer's protocol. After incubation with the CFSE working solution in the dark, staining was quenched by adding serum-containing medium. Cells were washed, replated, and treated with IAA, PA, or PA + IAA according to the experimental design.

At the end of treatment, cells were harvested, washed with PBS, and resuspended as single-cell suspensions. CFSE fluorescence was detected using a BD FACSCanto™ II flow cytometer. Cell proliferation was evaluated based on CFSE fluorescence dilution and analyzed using FlowJo software.

Cell-cycle analysis

Cell-cycle distribution was determined by propidium iodide (PI) staining followed by flow cytometry. After treatment, KGN cells were harvested, washed with PBS, and fixed in precooled 70% ethanol at 4°C overnight. Before staining, cells were centrifuged to remove ethanol and washed with PBS. Cells were then stained using a Cell Cycle and Apoptosis Analysis Kit (Beyotime, Cat. No. C1052) according to the manufacturer's instructions.

PI fluorescence was acquired using a BD FACSCanto™ II flow cytometer. Cell aggregates and debris were excluded during gating, and cell-cycle distribution was analyzed using FlowJo software. Results were expressed as the percentage of cells in the G0/G1, S, and G2/M phases.

Intracellular ROS measurement

Intracellular reactive oxygen species (ROS) levels were detected using 2',7'-dichlorodihydrofluorescein diacetate (DCFH-DA; Beyotime, Cat. No. S0033S). After treatment, culture medium was removed, and cells were washed twice with PBS. Cells were incubated with 10 μM DCFH-DA working solution at 37°C for 30 min in the dark. After incubation, cells were washed three times with PBS to remove extracellular probe, detached with trypsin, collected by centrifugation, and resuspended in PBS as single-cell suspensions.

The fluorescence of oxidized DCF was measured using the FITC channel on a BD FACSCanto™ II flow cytometer. Dead cells and debris were excluded during analysis, and intracellular ROS levels were quantified as mean fluorescence intensity using FlowJo software.

In vitro assessment of IAA production by Bacteroides fragilis

To determine whether *Bacteroides fragilis* produces indole-3-acetic acid (IAA), the strain was cultured under anaerobic conditions in the presence or absence of L-tryptophan (L-Trp), a precursor for microbial IAA biosynthesis. *B. fragilis* was first expanded anaerobically to the logarithmic growth phase and then inoculated into fresh anaerobic medium at a 1:10 ratio. Four conditions were included: blank medium, blank medium supplemented with L-Trp, *B. fragilis*, and *B. fragilis* supplemented with L-Trp. L-Trp (MCE,

Cat. No. HY-N0623) was added at a final concentration of 1 mM. Cultures were incubated at 37°C under anaerobic conditions.

Culture supernatants were collected at 0 and 48 h. Bacterial cells were removed by centrifugation at 4°C, and the supernatants were subjected to methanol precipitation to remove proteins. After a second centrifugation, clarified supernatants were collected for IAA measurement. IAA concentrations were quantified using an enzyme-linked immunosorbent assay (ELISA) kit as described above, following the manufacturer's instructions.

RNA extraction and quantitative real-time PCR

After 48 h of IAA treatment, total RNA was extracted from KGN cells using TRIzol reagent (Invitrogen, Cat. No. 15596026). RNA concentration and purity were determined spectrophotometrically. Equal amounts of RNA were reverse-transcribed into complementary DNA (cDNA), followed by quantitative real-time polymerase chain reaction (qPCR) using a SYBR Green-based detection system. Relative messenger RNA (mRNA) expression was normalized to glyceraldehyde-3-phosphate dehydrogenase (GAPDH), and fold changes were calculated using the 2^−ΔΔCt method.

Western blot analysis

After the indicated treatments, KGN cells were harvested and lysed in radioimmunoprecipitation assay (RIPA) buffer supplemented with protease and phosphatase inhibitors to extract total protein. For experiments requiring subcellular fractionation, nuclear and cytoplasmic proteins were isolated separately before immunoblotting. Protein concentrations were determined using a bicinchoninic acid (BCA) assay.

Equal amounts of protein were separated by sodium dodecyl sulfate-polyacrylamide gel electrophoresis (SDS-PAGE) and transferred onto polyvinylidene fluoride (PVDF) membranes. Membranes were blocked with 5% non-fat milk or bovine serum albumin (BSA) and incubated with primary antibodies at dilutions recommended by the manufacturers. The following primary antibodies were used: AHR (Proteintech, Cat. No. 67785-1-Ig), P21 (Proteintech, Cat. No. 10355-1-AP), P27 (Proteintech, Cat. No. 25614-1-AP), Cyclin D1 (Proteintech, Cat. No. 26939-1-AP), Cyclin E1 (Proteintech, Cat. No. 11554-1-AP), phosphorylated Rb (p-Rb; Proteintech, Cat. No. 87211-3-RR), total Rb (Proteintech, Cat. No. 17218-1-AP), E2F1 (Proteintech, Cat. No. 12171-1-AP), CHOP (Proteintech, Cat. No. 15204-1-AP), GAPDH (Proteintech, Cat. No. 60004-1-Ig), and Histone H3.

After washing, membranes were incubated with horseradish peroxidase (HRP)-conjugated secondary antibodies. Protein bands were visualized using an enhanced chemiluminescence (ECL) detection system. Densitometric analysis was performed using ImageJ software. For total cellular proteins, target protein abundance was normalized to GAPDH. For subcellular fractionation experiments, cytoplasmic proteins were normalized to GAPDH, whereas nuclear proteins were normalized to Histone H3.

Metabolomic analysis

Untargeted metabolomic profiling was performed by Shanghai Yuanxin Biotechnology Co., Ltd. Fecal samples were analyzed using liquid chromatography-mass spectrometry (LC-MS). Briefly, metabolites were extracted from fecal samples, subjected to chromatographic separation, and detected by mass spectrometry under standardized quality-control procedures. Raw LC-MS data were processed for peak detection, alignment, normalization, and metabolite annotation.

Multivariate statistical analyses, including principal component analysis (PCA) and partial least-squares discriminant analysis (PLS-DA), were performed to assess global metabolic differences among groups. Differential metabolites were identified based on the combined criteria of multivariate model contribution and univariate statistical testing. Pathway enrichment analysis was performed for annotated differential metabolites where applicable.

16S rRNA gene sequencing and microbiota analysis

Fecal microbiota profiling was performed by Shanghai Yuanxin Biotechnology Co., Ltd. Although initially designed to assess microbial community alterations, this analysis was based on 16S ribosomal RNA (rRNA) gene sequencing rather than shotgun metagenomic sequencing. Microbial genomic DNA was extracted from fecal samples and subjected to high-throughput sequencing of the bacterial 16S rRNA gene.

Sequencing data were processed using QIIME-based bioinformatic pipelines. After quality filtering, denoising or clustering, and removal of low-quality reads, representative sequences were taxonomically assigned against a reference microbial database. Alpha diversity and beta diversity analyses were performed to evaluate within-sample diversity and between-group community dissimilarity, respectively. Differences in microbial composition among groups were further analyzed at different taxonomic levels, and potential associations between microbial taxa and host metabolic or reproductive phenotypes were explored where appropriate.

Transcriptomic analysis

KGN cells from the IAA-treated and control groups were collected after treatment, and total RNA was extracted using TRIzol reagent (Invitrogen, Cat. No. 15596026). RNA sequencing was performed by Wuhan iGeneBook Biotechnology Co., Ltd. RNA integrity and concentration were assessed before library construction. Qualified RNA samples were used to generate sequencing libraries, followed by high-throughput sequencing on an Illumina platform.

Raw sequencing reads were subjected to quality control to remove adapters and low-quality reads. Clean reads were aligned to the human reference genome, and gene-level expression abundance was quantified. Differentially expressed genes between the IAA-treated and control groups were identified using DESeq2. Functional enrichment analyses, including Gene Ontology (GO) and Kyoto Encyclopedia of Genes and Genomes (KEGG) pathway analyses, were performed to identify biological processes and signaling pathways associated with IAA treatment.

Statistical analysis

Statistical analyses were performed using GraphPad Prism 8. For *in vitro* experiments, data were obtained from at least three independent experiments unless otherwise stated. For animal and clinical analyses, the number of biological replicates is indicated in the corresponding figure legends. Data from in vitro and animal experiments are presented as mean ± standard error of the mean (SEM) or mean ± standard deviation (SD), as appropriate. Clinical characteristics are presented as median with interquartile range (IQR) and were compared using the Mann–Whitney *U* test.

For comparisons between two groups, normally distributed data were analyzed using an unpaired two-tailed Student's *t*-test, whereas non-normally distributed data were analyzed using the Mann–Whitney U test. Comparisons among multiple groups were performed using one-way analysis of variance (ANOVA), followed by Tukey's honestly significant difference (HSD) post hoc test when appropriate. A value of $P < 0.05$ was considered statistically significant.

Results

Gut microbiota and metabolic profiles are altered in women with polycystic ovary syndrome and overweight/obesity

We first enrolled reproductive-aged women with overweight/obesity, defined by a body mass index (BMI) ≥ 24 kg/m², who met the predefined inclusion and exclusion criteria. The clinical characteristics of the participants are shown in Fig. 1A. Age and BMI were comparable between the control and polycystic ovary syndrome (PCOS) groups, minimizing the potential confounding effects of these two variables. As expected, women with PCOS showed higher luteinizing hormone (LH) levels and an increased LH/follicle-stimulating hormone (FSH) ratio, whereas FSH levels did not differ significantly between groups. Serum testosterone levels also differed between the two groups, consistent with the endocrine disturbance characteristic of PCOS.

To define the gut microbial features associated with PCOS in this cohort, fecal microbiota composition was profiled by 16S rRNA gene sequencing. Alpha diversity did not differ significantly between the control and PCOS groups (Fig. 1B,C), indicating that within-sample microbial diversity was largely preserved. In contrast, beta diversity analysis revealed a clear separation in microbial community structure between groups (Fig. 1D; Adonis, $R^2 = 0.183$, $P = 0.001$), suggesting that PCOS was associated with a compositional shift in the gut microbiota rather than a simple loss of microbial diversity.

We next performed LEfSe analysis to identify taxa contributing to the observed compositional differences. Several taxa showed differential enrichment between groups (Fig. 1E). *Bacteroides fragilis*, *Bacteroides stercoris*, and *Phocaeicola vulgatus* were enriched in the PCOS group, whereas *Faecalibacterium*, *Agathobacter rectalis*, and *Roseburia inulinivorans* were more abundant in controls.

These findings point to a disease-associated restructuring of the gut microbial ecosystem in women with PCOS and overweight/obesity.

Because shifts in gut microbiota are often accompanied by changes in microbial or host-microbial metabolites, we further performed fecal metabolomic profiling. PCA of fecal metabolomic profiles showed partial separation between the control and PCOS groups (Fig. 1F), indicating detectable differences in fecal metabolic signatures. Differential metabolites are shown in Fig. 1G; among these, indole-3-acetic acid (IAA), a tryptophan-derived indole metabolite, emerged as a metabolite of interest. To further identify metabolites contributing to group discrimination, an OPLS-DA model was constructed. S-plot analysis was used to evaluate metabolites contributing to group separation (Figure S1A), and permutation testing with 200 permutations was performed to assess the reliability of the model (Figure S1B).

These data show that women with PCOS and overweight/obesity harbor distinct gut microbial and fecal metabolic profiles. The enrichment of specific taxa together with altered indole-related metabolites suggests a potential microbiota-tryptophan metabolism axis associated with the PCOS phenotype.

Association and validation of gut microbial taxa and indole metabolites in PCOS

We next refined the microbiota and metabolomics datasets to identify candidate taxa and metabolites linked to the PCOS-associated signature. Species-level comparison revealed a distinct set of differentially abundant taxa between the control and PCOS groups (Fig. 2A). Among these taxa, *B. fragilis* was significantly enriched in women with PCOS (Fig. 2B), consistent with the taxonomic shift observed in the overall microbial community.

We then examined whether this microbial alteration was accompanied by changes in related metabolic pathways. KEGG enrichment analysis showed that the differential metabolites were preferentially associated with indole-related metabolism (Fig. 2C). At the metabolite level, IAA was significantly increased in the PCOS group (Fig. 2D), further focusing attention on tryptophan-derived indole metabolism.

To connect the microbial and metabolic features more directly, we analyzed the relationship between *B. fragilis* abundance and IAA levels. *B. fragilis* showed a positive correlation with IAA (Fig. 2E). Consistently, microbe-metabolite network analysis placed *B. fragilis* and IAA within the same connected module (Fig. 2F), supporting a coordinated alteration of this bacterial species and its associated indole metabolite in PCOS.

We further validated these findings using targeted assays. qPCR confirmed the increased abundance of *B. fragilis* in the PCOS group (Fig. 2G). Measurement of IAA in clinical samples showed that IAA was elevated not only in serum but also in follicular fluid from women with PCOS (Fig. 2H,I). These results

indicate that the increase in IAA extends beyond the intestinal metabolic profile and is also reflected in the systemic circulation and ovarian follicular microenvironment.

Together, these data identify a coordinated increase in *B. fragilis* and IAA in PCOS, highlighting a potential gut microbial-indole metabolite axis associated with the disease phenotype.

Functional assessment of the B. fragilis-IAA axis in PCOS

Given the coordinated increase in *B. fragilis* and IAA in women with PCOS, we next asked whether this microbe-metabolite association was reflected in the ovarian microenvironment. IAA levels in serum were positively correlated with those in follicular fluid (Fig. 3A), indicating that systemic IAA abundance is linked to IAA levels within the follicular milieu.

We then examined whether *B. fragilis* could contribute directly to IAA production. When cultured in the presence of L-tryptophan, *B. fragilis* produced higher levels of IAA in vitro (Fig. 3B), supporting its capacity to generate this tryptophan-derived indole metabolite. To determine whether this alteration was specific to IAA or represented a broader disturbance in indole-related metabolism, we quantified additional indole derivatives in paired clinical samples. In serum, indole-3-propionic acid (IPA), 5-hydroxytryptamine (5-HT), and melatonin (MT) did not differ significantly between the control and PCOS groups (Fig. 3C-E). The same pattern was observed in follicular fluid, where IPA, 5-HT, and MT remained comparable between groups (Fig. 3F-H). In contrast, IAA was consistently increased in PCOS, identifying IAA as the predominant indole-related metabolite altered in this cohort.

We next tested whether elevation of this bacterium or metabolite alone was sufficient to perturb ovarian function in vivo. Under the current intervention conditions, neither *B. fragilis* administration nor IAA treatment induced overt ovarian abnormalities. Histological examination showed no obvious changes in ovarian morphology (Fig. 3I), and follicle counts were comparable among groups (Fig. 3J). Estrous cycle monitoring likewise revealed no significant disruption of cyclicity (Fig. 3K, Figure S2A).

These findings indicate that although *B. fragilis* is capable of producing IAA and IAA is selectively increased in serum and follicular fluid from women with PCOS, isolated exposure to *B. fragilis* or IAA does not appear sufficient to induce a PCOS-like ovarian phenotype. In the context of an overweight/obesity-enriched clinical cohort, this result suggests that the functional impact of the *B. fragilis*-IAA axis may depend on an accompanying metabolic stress state.

High-fat diet enables the pathogenic effect of B. fragilis in PCOS-like ovarian dysfunction

The absence of an overt phenotype after *B. fragilis* or IAA exposure alone led us to test whether a metabolically stressed host environment was required for this axis to affect ovarian function. We therefore combined *B. fragilis* administration with HFD feeding and examined reproductive and metabolic phenotypes.

Ovarian morphology was assessed by H&E staining (Fig. 4A). Compared with control mice, mice receiving HFD together with *B. fragilis* displayed ovarian abnormalities resembling PCOS, including disrupted follicular development. Quantitative follicle analysis confirmed a marked shift in follicular composition in the HFD + *B. fragilis* group (Fig. 4B), indicating impaired folliculogenesis under combined microbial and metabolic stress.

We next examined whether this phenotype was accompanied by changes in indole-related metabolites. Serum IAA levels were significantly increased in the HFD + *B. fragilis* group, whereas IPA, 5-HT, and MT remained unchanged (Fig. 4C-F). This pattern mirrored the clinical findings and suggested a selective increase in IAA rather than a broad disturbance in indole metabolism.

Consistent with the ovarian phenotype, endocrine profiling revealed a PCOS-like hormonal disturbance in the HFD + *B. fragilis* group. Testosterone and LH levels were elevated, accompanied by an increased LH/FSH ratio, whereas FSH and E2 levels were reduced (Fig. 4G-K). Estrous cycle monitoring further showed disrupted cyclicity in this group (Fig. 4L), supporting functional impairment of the hypothalamic-pituitary-ovarian axis.

Because the phenotype emerged in the context of HFD feeding, we also evaluated metabolic parameters. As expected, HFD-fed mice showed increased body weight, inguinal fat mass, and inguinal fat-to-body weight ratio (Figure S2B-D). Histological assessment of adipose tissue further revealed adipocyte hypertrophy and increased lipid accumulation, as reflected by enlarged adipocyte size and stronger Oil Red O staining (Figure S2E,F).

These results indicate that *B. fragilis* exerts a pathogenic effect on ovarian function only in the presence of diet-induced metabolic stress. The accompanying selective elevation of IAA supports a context-dependent role of the *B. fragilis*-IAA axis in promoting PCOS-like reproductive and endocrine abnormalities.

IAA mediates PCOS-like phenotypes under metabolic stress

Having established that *B. fragilis* promoted PCOS-like abnormalities only in the presence of HFD-induced metabolic stress, we next asked whether IAA itself could reproduce these effects under the same metabolic context.

To test this, mice were treated with IAA during HFD feeding. Ovarian morphology was first examined by H&E staining (Fig. 5A). Compared with control mice, the HFD + IAA group displayed ovarian features consistent with PCOS-like dysfunction, including disrupted follicular development and altered ovarian architecture. Quantitative follicle analysis further confirmed changes in follicular composition in the HFD + IAA group (Fig. 5B).

These structural changes were accompanied by endocrine abnormalities. Testosterone and LH levels were increased in HFD + IAA-treated mice, together with an elevated LH/FSH ratio. In contrast, FSH and E2 levels were reduced (Fig. 5C-G). Estrous cycle monitoring further revealed disrupted cyclicity in the HFD + IAA group (Fig. 5H), indicating impaired reproductive function.

These results show that IAA is sufficient to induce PCOS-like ovarian, endocrine, and estrous cycle abnormalities in the setting of HFD-induced metabolic stress. Together with the *B. fragilis* intervention data, these findings support IAA as a functional metabolite linking *B. fragilis* enrichment to PCOS-like phenotypes under metabolically challenged conditions.

IAA impairs granulosa cell proliferation and activates AHR signaling

We next investigated how IAA affects granulosa cells at the cellular level. KGN cells were exposed to increasing concentrations of IAA, and cell viability was first assessed using the CCK-8 assay. IAA did not cause significant cytotoxicity at concentrations up to 40 μM (Figure S3A), allowing subsequent functional analyses to be performed within a non-cytotoxic range.

To define the transcriptional response to IAA, RNA sequencing (RNA-seq) was performed. Differentially expressed genes were prominently enriched in pathways related to cell-cycle regulation and apoptosis (Fig. 6A), a pattern also observed in supplementary enrichment analysis (Figure S3B). Among the downregulated genes, several central regulators of cell-cycle progression, including *E2F1*, *PLK1*, and *CDC20*, ranked among the most affected transcripts (Fig. 6B). Heatmap visualization and gene set enrichment analysis (GSEA) further showed coordinated suppression of cell cycle-associated gene expression after IAA treatment (Fig. 6C,D), suggesting that IAA restrains cell-cycle progression in granulosa cells. Apoptosis-related transcriptional changes were also detected (Figure S3C,D), indicating that IAA elicits a broader stress-associated response.

Functional assays confirmed the transcriptional findings. Flow cytometry revealed accumulation of cells in the G0/G1 phase and a reduction in the G2/M population after IAA treatment (Fig. 6E,F). CFSE dilution assays showed reduced proliferative capacity following IAA exposure (Fig. 6G,H), indicating that IAA suppresses granulosa cell proliferation primarily by limiting cell-cycle progression.

Because indole derivatives can act as ligands for the aryl hydrocarbon receptor (AHR)[33, 34], we examined whether AHR signaling was engaged by IAA. Both qPCR and Western blot analyses showed increased AHR expression after IAA treatment (Fig. 6I,J), implicating AHR activation as a potential mechanism underlying the anti-proliferative effect of IAA.

Lipotoxic stress potentiates IAA-induced AHR activation and cell-cycle arrest

We next asked whether a lipid-rich metabolic environment could amplify the cellular effects of IAA. KGN cells were exposed to palmitic acid (PA)-induced lipotoxic stress, either alone or in combination with IAA.

Compared with either treatment alone, combined PA and IAA exposure caused a more pronounced accumulation of cells in the G0/G1 phase (Fig. 7A,B), indicating that lipotoxic stress enhances the ability of IAA to restrain cell-cycle progression.

We then examined AHR activation under these conditions. Combined PA and IAA treatment markedly increased nuclear accumulation of AHR compared with single treatments (Fig. 7C,D), suggesting enhanced activation of AHR signaling in the lipotoxic context. Consistent with the observed G0/G1 arrest, analysis of cell-cycle regulatory proteins showed increased expression of p21 and p27, accompanied by reduced levels of Cyclin D1, Cyclin E1, phosphorylated Rb (p-Rb), and E2F1 (Fig. 7E,F). These changes indicate suppression of the Cyclin D/E-Rb-E2F axis and inhibition of G1/S transition.

To determine whether AHR signaling contributed to this response, AHR was pharmacologically inhibited or genetically knocked down. Suppression of AHR partially reversed the PA + IAA-induced changes in cell-cycle distribution and cell-cycle regulatory protein expression (Fig. 7G,H), indicating that AHR is required for mediating IAA-induced cell-cycle arrest under lipotoxic stress.

We further assessed the cellular stress response induced by PA exposure. PA increased intracellular reactive oxygen species (ROS) levels and upregulated C/EBP homologous protein (CHOP) expression (Fig. 7K), consistent with oxidative and endoplasmic reticulum stress. These stress signals may sensitize granulosa cells to IAA-induced AHR activation and cell-cycle inhibition.

Together, these findings show that lipotoxic stress potentiates the anti-proliferative effect of IAA in granulosa cells. Under these conditions, IAA activates AHR signaling and suppresses G1/S progression through regulation of the p21/p27-Cyclin D/E-Rb-E2F1 axis.

Discussion

This study identifies a context-dependent gut microbiota-metabolite mechanism that links metabolic stress to PCOS-like ovarian dysfunction. By integrating clinical microbiota and metabolomic profiling with in vivo and in vitro validation, we show that *Bacteroides fragilis* is enriched in women with PCOS and overweight/obesity and is associated with increased IAA. IAA was elevated not only in fecal metabolic profiles but also in serum and follicular fluid, placing this metabolite at the interface between the gut microbial compartment, systemic circulation, and the ovarian follicular microenvironment. Functionally, neither *B. fragilis* nor IAA alone was sufficient to induce overt ovarian abnormalities under basal conditions. In contrast, under HFD-induced metabolic stress, both *B. fragilis* and IAA promoted PCOS-like reproductive and endocrine phenotypes. Mechanistically, IAA suppressed granulosa cell proliferation through AHR-dependent inhibition of G1/S cell-cycle progression, an effect that was amplified by lipotoxic stress. These findings support a model in which the *B. fragilis*-IAA-AHR axis acts as a metabolic stress-dependent contributor to ovarian dysfunction.

Gut microbiota dysbiosis has been increasingly implicated in PCOS, with reported associations between altered microbial communities and hyperandrogenism, insulin resistance, chronic inflammation, and metabolic dysfunction[35, 36]. However, many human studies remain descriptive, and the reported

microbial signatures are not always consistent across cohorts, likely reflecting differences in ethnicity, body mass index, diet, medication exposure, diagnostic criteria, and sequencing strategy[37]. A major challenge in the field is therefore to move beyond community-level associations and define specific microbial species, metabolites, and host pathways that are functionally relevant to disease biology. Our study addresses this gap by focusing on a defined microbe-metabolite pair. The enrichment of *B. fragilis*, its positive association with IAA, and its capacity to generate IAA in vitro provide a plausible microbial source for the altered indole metabolite profile observed in PCOS. More importantly, the in vivo data indicate that this association has functional consequences, but only within a metabolically challenged host environment.

A notable observation is that IAA emerged as the predominant altered indole-related metabolite in this cohort. Previous studies of microbiota-derived metabolites in PCOS have largely emphasized short-chain fatty acids, bile acids, branched-chain amino acid metabolism, and inflammatory mediators[38–40]. Indole derivatives have received less attention, despite their established roles as host-microbe signaling molecules[41]. IAA is generated from tryptophan metabolism by specific gut bacteria and can modulate host physiology through several pathways, including AHR signaling[42]. In our clinical samples, IAA was increased in PCOS, whereas indole-3-propionic acid, 5-hydroxytryptamine, and melatonin were not consistently altered. This selectivity argues against a generalized disturbance of indole metabolism and instead suggests a more specific remodeling of the tryptophan-IAA branch. The elevation of IAA in follicular fluid is particularly relevant, as the follicular microenvironment directly shapes granulosa cell function, oocyte competence, and follicular development. Thus, gut-derived or gut-associated metabolites may influence ovarian physiology not only through systemic metabolic inflammation but also through direct changes in the biochemical composition of follicular fluid.

The context-dependent effect of *B. fragilis* and IAA is central to the interpretation of this work. Under basal conditions, isolated exposure to either *B. fragilis* or IAA did not induce a PCOS-like phenotype, indicating that this axis is not intrinsically sufficient to disrupt ovarian function in an otherwise unstressed host. In contrast, HFD feeding enabled both *B. fragilis* and IAA to promote ovarian morphological abnormalities, endocrine disruption, and estrous cycle irregularity. This finding is consistent with the multifactorial nature of PCOS, in which genetic susceptibility, diet, adiposity, insulin resistance, inflammation, and environmental exposures converge to shape disease onset and severity[43, 44]. It also provides a framework for understanding why microbiota alterations alone may not uniformly predict PCOS across populations. Rather than acting as a primary driver in isolation, the gut microbiota may function as a disease amplifier whose impact becomes evident under permissive metabolic conditions. In this sense, the *B. fragilis*-IAA axis may represent a microbial “second hit” that aggravates ovarian dysfunction in the setting of diet-induced metabolic stress.

At the cellular level, our data identify impaired granulosa cell proliferation as a downstream consequence of IAA exposure. Granulosa cells are essential for follicular growth, steroidogenesis, oocyte support, and follicle selection. Defective granulosa cell proliferation and survival are closely linked to follicular arrest, a hallmark of PCOS ovarian pathology[45]. RNA-seq analysis revealed that IAA broadly suppressed cell

cycle-associated transcriptional programs, including key regulators such as *E2F1*, *PLK1*, and *CDC20*. Functional assays confirmed accumulation of cells in G0/G1 and reduced proliferative capacity. These findings were further supported by changes in canonical G1/S regulators, including increased p21 and p27 and reduced Cyclin D1, Cyclin E1, phosphorylated Rb, and E2F1. Together, these data place the G1/S checkpoint as a major cellular target of IAA in granulosa cells.

AHR provides a mechanistic link between IAA exposure and granulosa cell-cycle arrest. AHR is a ligand-activated transcription factor that senses environmental chemicals, dietary compounds, and microbiota-derived metabolites. It has been implicated in xenobiotic metabolism, immune regulation, barrier function, and reproductive biology[46]. Our results show that IAA increased AHR expression and promoted AHR nuclear accumulation, particularly under lipotoxic conditions. Pharmacological inhibition or knockdown of AHR partially reversed the IAA-induced cell-cycle phenotype and restored the expression of key cell-cycle proteins, supporting a causal role for AHR signaling. The partial nature of the rescue is biologically informative. It suggests that AHR is a major mediator of IAA action but may not be the only pathway involved. IAA may also engage additional metabolic, oxidative stress, or mitochondrial pathways that converge on granulosa cell proliferation.

The interaction between lipotoxic stress and IAA-induced AHR activation may explain why the in vivo phenotype required HFD exposure. Palmitic acid increased intracellular reactive oxygen species and CHOP expression, indicating oxidative and endoplasmic reticulum stress. These stress signals can alter cellular redox state, transcriptional responsiveness, and checkpoint control, thereby sensitizing granulosa cells to external metabolic cues. In PCOS, obesity and insulin resistance are frequently accompanied by oxidative stress, low-grade inflammation, and lipotoxic injury within ovarian tissue[47]. Our data suggest that under such conditions, IAA-AHR signaling becomes more detrimental, shifting granulosa cells toward cell-cycle arrest and impaired proliferation. This provides a mechanistic basis for a two-hit model: metabolic stress primes the ovarian cellular environment, while microbiota-associated IAA drives AHR-dependent suppression of granulosa cell proliferation.

These findings also refine the emerging concept of the gut-ovary axis. The gut microbiota has often been linked to PCOS through systemic metabolic inflammation, insulin resistance, or androgen regulation. Our study adds another layer by showing that a specific microbial metabolite is increased in follicular fluid and can directly alter granulosa cell biology. This does not exclude broader systemic mechanisms; rather, it suggests that gut microbial signals may influence ovarian function through both indirect metabolic effects and direct actions within the follicular niche. From a translational perspective, the data raise the possibility that targeting microbial tryptophan metabolism, limiting IAA accumulation, or modulating AHR signaling could be explored as intervention strategies for metabolically complicated PCOS. Such approaches would require caution, as both indole metabolites and AHR signaling have ligand-, tissue-, and context-dependent effects. The therapeutic goal may not be complete suppression of this pathway, but restoration of a balanced microbial and metabolic state.

Several limitations should be acknowledged. First, although the study combines clinical samples with experimental validation, the clinical cohort remains relatively limited. Larger and more diverse cohorts will be needed to determine whether the *B. fragilis*-IAA signature is specific to women with PCOS and overweight/obesity or extends to other PCOS phenotypes. Second, IAA was measured in serum and follicular fluid, but flux from the gut to the ovarian compartment was not directly traced. Stable isotope-based approaches could help establish the contribution of microbial tryptophan metabolism to circulating and follicular IAA pools. Third, although *B. fragilis* produced IAA in vitro and reproduced PCOS-like phenotypes under HFD conditions, strain-level differences in *B. fragilis* biology were not addressed. Given the functional heterogeneity of this species, future studies should determine whether specific strains or gene modules are responsible for IAA production and ovarian effects. Fourth, AHR inhibition and knockdown support a mechanistic role for AHR in granulosa cells, but downstream transcriptional targets and possible crosstalk with oxidative stress, insulin signaling, steroidogenesis, and mitochondrial function remain to be defined. Finally, PCOS is a heterogeneous disorder, and additional microbial species, metabolites, and host pathways are likely to cooperate with the *B. fragilis*-IAA axis in shaping disease phenotypes.

This work defines a metabolically gated mechanism by which *B. fragilis*-associated IAA contributes to PCOS-like ovarian dysfunction. The data support a model in which HFD-induced metabolic stress sensitizes granulosa cells to IAA, leading to AHR activation, suppression of the p21/p27-Cyclin D/E-Rb-E2F1 cell-cycle axis, impaired granulosa cell proliferation, and consequent disruption of follicular development. By linking a specific gut microbial species, a tryptophan-derived metabolite, and an ovarian cellular pathway, these findings provide mechanistic insight into how the gut microbiota may aggravate PCOS in the setting of metabolic stress.

Declarations

Data availability

The RNA-seq data generated in this study have been deposited in the Gene Expression Omnibus (GEO) under accession number GSE328499. The metagenomic sequencing data have been deposited in the NCBI BioProject database under accession number PRJNA1453510. Other data supporting the findings of this study are available from the corresponding author upon reasonable request.

Ethics declarations

Clinical trial number: not applicable.

This study, including the collection and use of human samples and all animal experiments, was approved by the Ethics Committee of The First Hospital of Lanzhou University (approval no. LDYYLL2024-257). Written informed consent was obtained from all participants prior to enrollment and sample collection. All procedures involving human participants were performed in accordance with the ethical standards of the institutional research committee and with the 1964 Helsinki Declaration and its later amendments or

comparable ethical standards. All animal experiments were conducted in accordance with relevant institutional and national guidelines for the care and use of laboratory animals.

Consent for publication

All authors of this manuscript have consented to publication.

Competing interests

The authors declare that they have no competing interests.

Funding

This work was supported by the Gansu Provincial Joint Research Fund (Grant No. 25JRRA1240).

Author Contribution

Yan Wang, Conceptualization, Methodology, Investigation, Formal analysis, Data curation, Visualization, Writing–original draft. Zhijian Luo, Methodology, Validation, Investigation, Formal analysis, Data curation. Ting Yang, Investigation, Methodology, Data curation, Validation. Xiaorong Luo, Clinical sample collection, Investigation, Resources, Data curation. Xuehong Zhang-Conceptualization, Writing, review & editing, Supervision, Resources. All authors reviewed the manuscript.

Acknowledgements

We are grateful to all the people who helped us accomplish this project.

Data Availability

The RNA-sequencing data generated and analyzed during the current study are publicly available in the NCBI Gene Expression Omnibus (GEO) repository under accession number GSE328499.

References

1. Pililis S, Lampsas S, Kountouri A, Pliouta L, Korakas E, Livadas S, Thymis J, Peppa M, Kalantaridou S, Oikonomou E et al. The Cardiometabolic Risk in Women with Polycystic Ovarian Syndrome (PCOS): From Pathophysiology to Diagnosis and Treatment. Med (Kaunas) 2024, 60.
2. Zhao H, Zhang J, Cheng X, Nie X, He B. Insulin resistance in polycystic ovary syndrome across various tissues: an updated review of pathogenesis, evaluation, and treatment. J Ovarian Res. 2023;16:9.

3. Piltonen TT, Komsi E, Morin-Papunen LC, Korhonen E, Franks S, Järvelin MR, Arffman RK, Ollila MM. AMH as part of the diagnostic PCOS workup in large epidemiological studies. Eur J Endocrinol. 2023;188:547–54.
4. Bril F, Ezeh U, Amiri M, Hatoum S, Pace L, Chen YH, Bertrand F, Gower B, Azziz R. Adipose Tissue Dysfunction in Polycystic Ovary Syndrome. J Clin Endocrinol Metab. 2023;109:10–24.
5. Goldberg A, Graca S, Liu J, Rao V, Witchel SF, Pena A, Li R, Mousa A, Tay CT, Pattuwage L, et al. Anti-obesity pharmacological agents for polycystic ovary syndrome: A systematic review and meta-analysis to inform the 2023 international evidence-based guideline. Obes Rev. 2024;25:e13704.
6. Min Q, Geng H, Gao Q, Xu M. The association between gut microbiome and PCOS: evidence from meta-analysis and two-sample mendelian randomization. Front Microbiol. 2023;14:1203902.
7. Salehi S, Allahverdy J, Pourjafar H, Sarabandi K, Jafari SM. Gut Microbiota and Polycystic Ovary Syndrome (PCOS): Understanding the Pathogenesis and the Role of Probiotics as a Therapeutic Strategy. Probiotics Antimicrob Proteins. 2024;16:1553–65.
8. Fruzzetti F, Fidecicchi T, Benelli E, Baldari F, Tonacchera M. Body mass index is a good predictor of metabolic abnormalities in polycystic ovary syndrome. J Endocrinol Invest. 2024;47:927–36.
9. Lonardo MS, Cacciapuoti N, Guida B, Di Lorenzo M, Chiurazzi M, Damiano S, Menale C. Hypothalamic-Ovarian axis and Adiposity Relationship in Polycystic Ovary Syndrome: Physiopathology and Therapeutic Options for the Management of Metabolic and Inflammatory Aspects. Curr Obes Rep. 2024;13:51–70.
10. Zheng C, Lin Y, Zhang Z, Ye J, Lin Y, Tian J. Analyzing and evaluating the metabolic and endocrine characteristics between lean and obese patients with polycystic ovary syndrome: a systemic review and meta-analysis. Front Endocrinol (Lausanne). 2025;16:1680685.
11. Li XL, Ji YF, Feng Y, Liu SW. Metabolic disparities between obese and non-obese patients with polycystic ovary syndrome: implications for endometrial receptivity indicators. Gynecol Endocrinol. 2024;40:2312895.
12. López-Alarcón M, Vital-Reyes VS, Almeida-Gutiérrez E, Maldonado-Hernández J, Flores-Chávez S, Domínguez-Salgado JM, Vite-Bautista J, Cruz-Martínez D. Barradas-Vázquez AS, Z'Cruz-López R: Obesity and Hyperandrogenemia in Polycystic Ovary Syndrome: Clinical Implications. J Pers Med 2023, 13.
13. Kim JJ. Obesity and Polycystic Ovary Syndrome. J Obes Metab Syndr. 2024;33:289–301.
14. Li M, Chi X, Wang Y, Setrerrahmane S, Xie W, Xu H. Trends in insulin resistance: insights into mechanisms and therapeutic strategy. Signal Transduct Target Ther. 2022;7:216.
15. Helvaci N, Yildiz BO. Polycystic ovary syndrome as a metabolic disease. Nat Rev Endocrinol. 2025;21:230–44.
16. Stefanaki K, Karagiannakis DS, Peppa M, Vryonidou A, Kalantaridou S, Goulis DG, Psaltopoulou T, Paschou SA. Food Cravings and Obesity in Women with Polycystic Ovary Syndrome: Pathophysiological and Therapeutic Considerations. Nutrients 2024, 16.
17. Saad MJA, Santos A. The Microbiota and Evolution of Obesity. Endocr Rev. 2025;46:300–16.

18. Robinson JM, Wissel EF, Breed MF. Policy implications of the microbiota-gut-brain axis. Trends Microbiol. 2024;32:107–10.
19. Li P, Xie L, Zheng H, Feng Y, Mai F, Tang W, Wang J, Lan Z, Lv S, Jayawardana T, et al. Gut microbial-derived 3,4-dihydroxyphenylacetic acid ameliorates reproductive phenotype of polycystic ovary syndrome. Imeta. 2025;4:e70065.
20. Wu J, Wang K, Qi X, Zhou S, Zhao S, Lu M, Nie Q, Li M, Han M, Luo X, et al. The intestinal fungus Aspergillus tubingensis promotes polycystic ovary syndrome through a secondary metabolite. Cell Host Microbe. 2025;33:119–e136111.
21. Geng L, Yang X, Sun J, Ran X, Zhou D, Ye M, Wen L, Wang R, Chen M. Gut Microbiota Modulation by Inulin Improves Metabolism and Ovarian Function in Polycystic Ovary Syndrome. Adv Sci (Weinh). 2025;12:e2412558.
22. de Castro Fonseca M, Zanetti L, Fanourakis S, Sulzer DL, Mazmanian SK. The gut microbiome, systemic inflammation, and autoimmunity in Parkinson's disease. Lancet Neurol. 2026;25:103–14.
23. Ohara TE, Hsiao EY. Microbiota-neuroepithelial signalling across the gut-brain axis. Nat Rev Microbiol. 2025;23:371–84.
24. Zhao C, Zhang Y, Chen K, Li Z, Chen L, Xing X, Geng H, Zheng Y, Zhang Y, Wang S et al. Sialic acid exacerbates polycystic ovary syndrome in mice by modulating gut microbiota-mediated bile acid metabolism and FXR activation. Nat Commun 2026.
25. Yang Y, Cheng J, Liu C, Zhang X, Ma N, Zhou Z, Lu W, Wu C. Gut microbiota in women with polycystic ovary syndrome: an individual based analysis of publicly available data. EClinicalMedicine. 2024;77:102884.
26. Zhang H, He Z, Chen Y, Chao J, Cheng X, Mao J, Chen Y, Li B, Yu J, Yan M, et al. Cordyceps polysaccharide improves polycystic ovary syndrome by inhibiting gut-derived LPS/TLR4 pathway to attenuates insulin resistance. Int J Biol Macromol. 2024;280:135844.
27. Zhang Y, Han X, Feng T, Li Z, Yu H, Chen Y, Gao Y, Gao Q, Zhang L, Li S, et al. Gut-microbiota-derived indole sulfate promotes heart failure in chronic kidney disease. Cell Host Microbe. 2025;33:1715–e17301715.
28. Serger E, Luengo-Gutierrez L, Chadwick JS, Kong G, Zhou L, Crawford G, Danzi MC, Myridakis A, Brandis A, Bello AT, et al. The gut metabolite indole-3 propionate promotes nerve regeneration and repair. Nature. 2022;607:585–92.
29. Collins SL, Stine JG, Bisanz JE, Okafor CD, Patterson AD. Bile acids and the gut microbiota: metabolic interactions and impacts on disease. Nat Rev Microbiol. 2023;21:236–47.
30. Lee JY, Mahan SP, Parente de Carvalho T, Nguyen H, Singai C, Camacho L, Tekeli M, Kwon YJ, Lee JW, Santos RL, et al. Host-derived nitrate fuels indole production by Escherichia coli to drive chronic kidney disease progression. Science. 2026;391:1250–5.
31. Bardhan P, Mei X, Lai NK, Mell B, Tummala R, Aryal S, Manandhar I, Hwang H, Jhuma TA, Atluri RR, et al. Salt-Responsive Gut Microbiota Induces Sex-Specific Blood Pressure Changes. Circ Res. 2024;135:1122–37.

32. Wang G, Fan Y, Zhang G, Cai S, Ma Y, Yang L, Wang Y, Yu H, Qiao S, Zeng X. Microbiota-derived indoles alleviate intestinal inflammation and modulate microbiome by microbial cross-feeding. Microbiome. 2024;12:59.
33. Coumoul X, Barouki R, Esser C, Haarmann-Stemmann T, Lawrence BP, Lehmann J, Moura-Alves P, Murray IA, Opitz CA, Perdew GH, Bourguet W. The aryl hydrocarbon receptor: structure, signaling, physiology and pathology. Signal Transduct Target Ther. 2026;11:20.
34. Stockinger B, Shah K, Wincent E. AHR in the intestinal microenvironment: safeguarding barrier function. Nat Rev Gastroenterol Hepatol. 2021;18:559–70.
35. Starling S. Key role for gut microbiota in PCOS development. Nat Rev Endocrinol. 2021;17:515.
36. Ramzan H, Bukhari DA, Bibi Z, Arifullah, Isha, Nawaz A, Rehman A. Probiotic supplement for the treatment of polycystic ovarian syndrome. Pharmacol Ther. 2025;266:108785.
37. Li P, Shuai P, Shen S, Zheng H, Sun P, Zhang R, Lan S, Lan Z, Jayawardana T, Yang Y, et al. Perturbations in gut microbiota composition in patients with polycystic ovary syndrome: a systematic review and meta-analysis. BMC Med. 2023;21:302.
38. He Y, Mei L, Wang L, Li X, Zhao J, Zhang H, Chen W, Wang G. Lactiplantibacillus plantarum CCFM1019 attenuate polycystic ovary syndrome through butyrate dependent gut-brain mechanism. Food Funct. 2022;13:1380–92.
39. Yun C, Yan S, Liao B, Ding Y, Qi X, Zhao M, Wang K, Zhuo Y, Nie Q, Ye C, et al. The microbial metabolite agmatine acts as an FXR agonist to promote polycystic ovary syndrome in female mice. Nat Metab. 2024;6:947–62.
40. Song J, Wang X, Feng D, Gao W, Wang X, Qiu X, Cheng W, Fang Y, Shi B, Li D. Exploration and analysis of methylglyoxal-driven chronic inflammation in polycystic ovary syndrome. J Adv Res. 2026;83:539–55.
41. Huang Z, Wells JM, Fogliano V, Capuano E. Microbial tryptophan catabolism as an actionable target via diet-microbiome interactions. Crit Rev Food Sci Nutr. 2025;65:3650–64.
42. Nie Q, Sun Y, Hu W, Chen C, Lin Q, Nie S. Glucomannan promotes Bacteroides ovatus to improve intestinal barrier function and ameliorate insulin resistance. Imeta. 2024;3:e163.
43. Dapas M, Dunaif A. Deconstructing a Syndrome: Genomic Insights Into PCOS Causal Mechanisms and Classification. Endocr Rev. 2022;43:927–65.
44. Peebles E, Wang Z, Dracup E, Sarcione C, Curry CL, Abrams K, Onnela JP, Williams MA, Hauser R, Coull B, Mahalingaiah S. Utilizing a digital cohort to understand the health burden and lifestyle characteristics across the life course in individuals with polycystic ovary syndrome and possible PCOS. Front Endocrinol (Lausanne). 2025;16:1585628.
45. Wang Y, Liu X, Li Z, Kang A, Bai Y, Wang Y, Liu Y, Zhang C, Yang J, Cai Q et al. Oligofructose alleviates hyperandrogenism in polycystic ovary syndrome through gut microbiota-derived bile acids. J Adv Res 2026.
46. Keskey RC, Xiao J, Hyoju S, Lam A, Kim D, Sidebottom AM, Zaborin A, Dijkstra A, Meltzer R, Thakur A, et al. Enterobactin inhibits microbiota-dependent activation of AhR to promote bacterial sepsis in

mice. Nat Microbiol. 2025;10:388–404.

47. Walter K. What Is Polycystic Ovary Syndrome? JAMA. 2022;327:294.

Figures

A

Variable	CON (n=8)	PCOS (n=8)	P value
Age (years)	30.5 (28.0–31.3)	30.5 (28.0–31.5)	0.958 ns
BMI (kg/m²)	29.5 (26.1–30.4)	27.4 (26.4–29.8)	1.000 ns
Testosterone (ng/ml)	0.28 (0.25–0.29)	0.50 (0.37–0.61)	0.002 **
FSH (IU/L)	6.04 (5.19–7.44)	4.88 (3.86–5.79)	0.105 ns
LH (IU/L)	5.01 (4.05–6.35)	13.60 (10.96–30.80)	0.002 **
LH/FSH	0.83 (0.64–1.18)	2.64 (2.20–6.37)	0.002 **

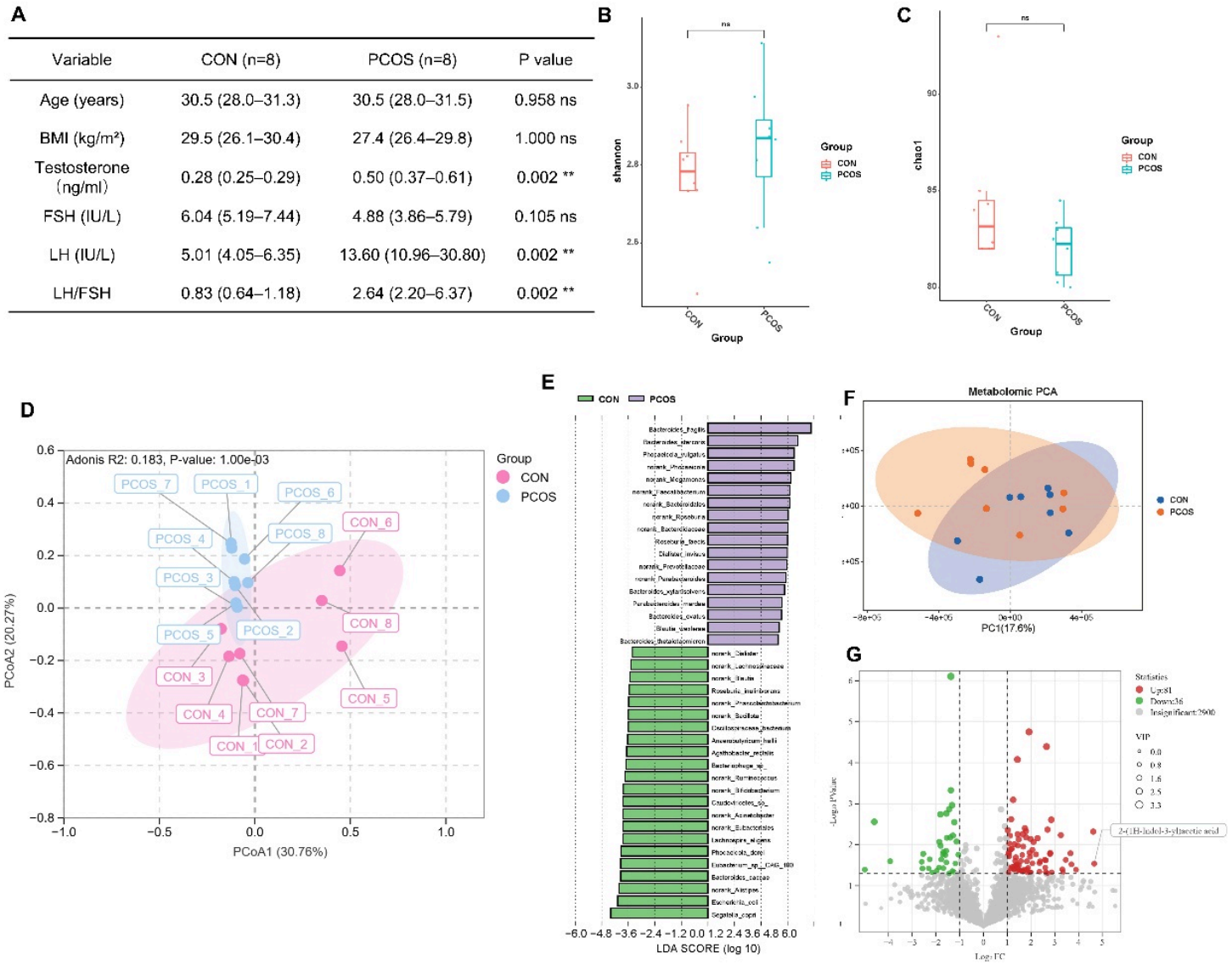


Figure 1

Gut microbiota and metabolic profiles are altered in women with polycystic ovary syndrome and overweight/obesity

(A) Baseline characteristics and hormone levels of study participants; (B, C) α-diversity analysis of gut microbiota; (D) β-diversity analysis based on principal coordinates analysis (PCoA); (E) LEfSe analysis showing differentially enriched taxa between groups; (F) Principal component analysis (PCA) of metabolomic profiles; (G) Volcano plot showing differential metabolites between groups.

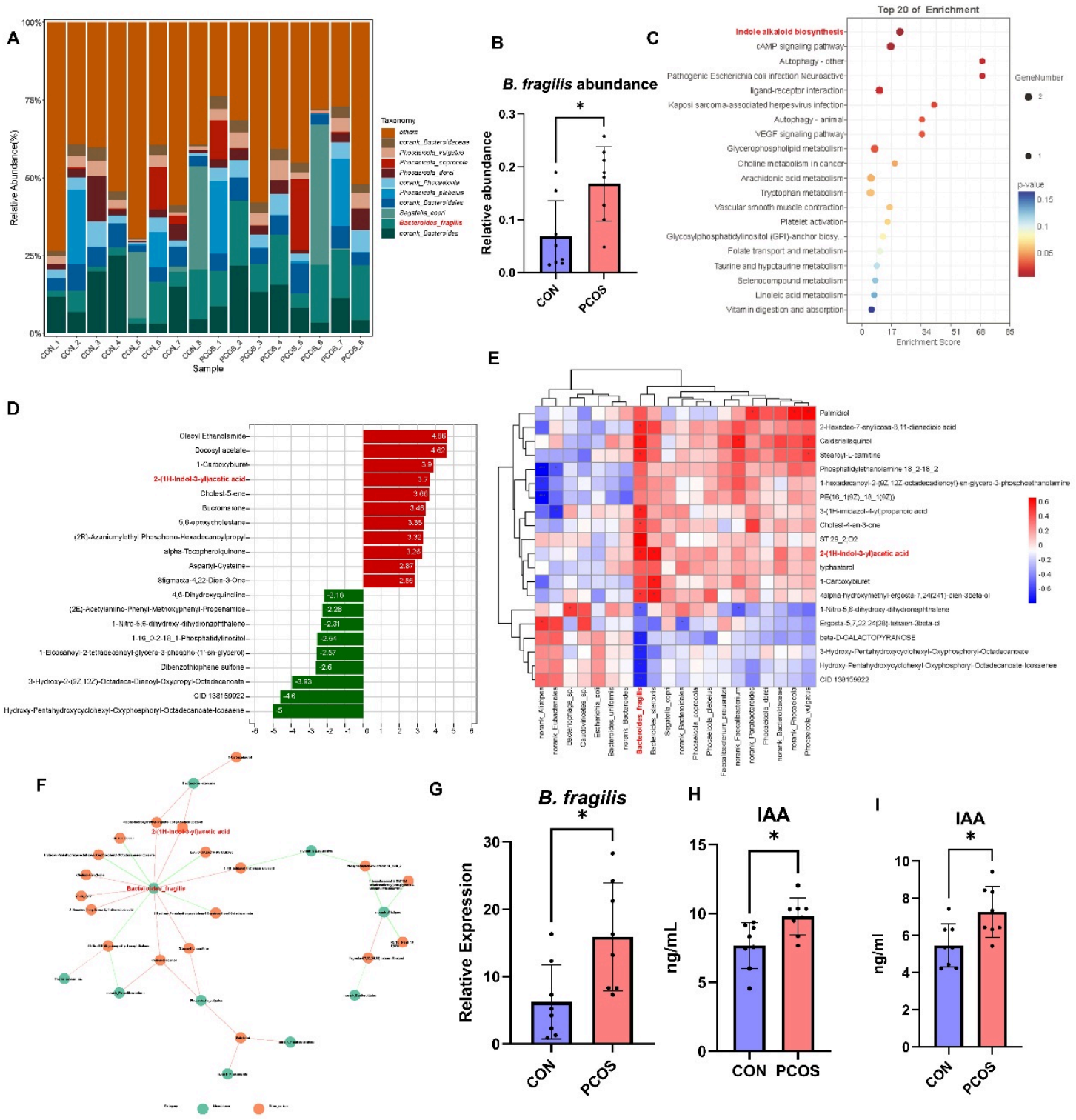


Figure 2

Association and validation of gut microbial taxa and indole metabolites in PCOS

(A) Species-level analysis of gut microbiota composition between groups; (B) Quantification of *Bacteroides fragilis* abundance; (C) KEGG enrichment analysis of differential metabolites; (D) Relative fecal levels of indole-3-acetic acid (IAA) between groups; (E) Correlation analysis between *Bacteroides*

fragilis and IAA; (F) Correlation network showing associations between *B. fragilis* and metabolites; (G) qPCR validation of *B. fragilis* abundance; (H, I) IAA levels in serum (H) and follicular fluid (I).

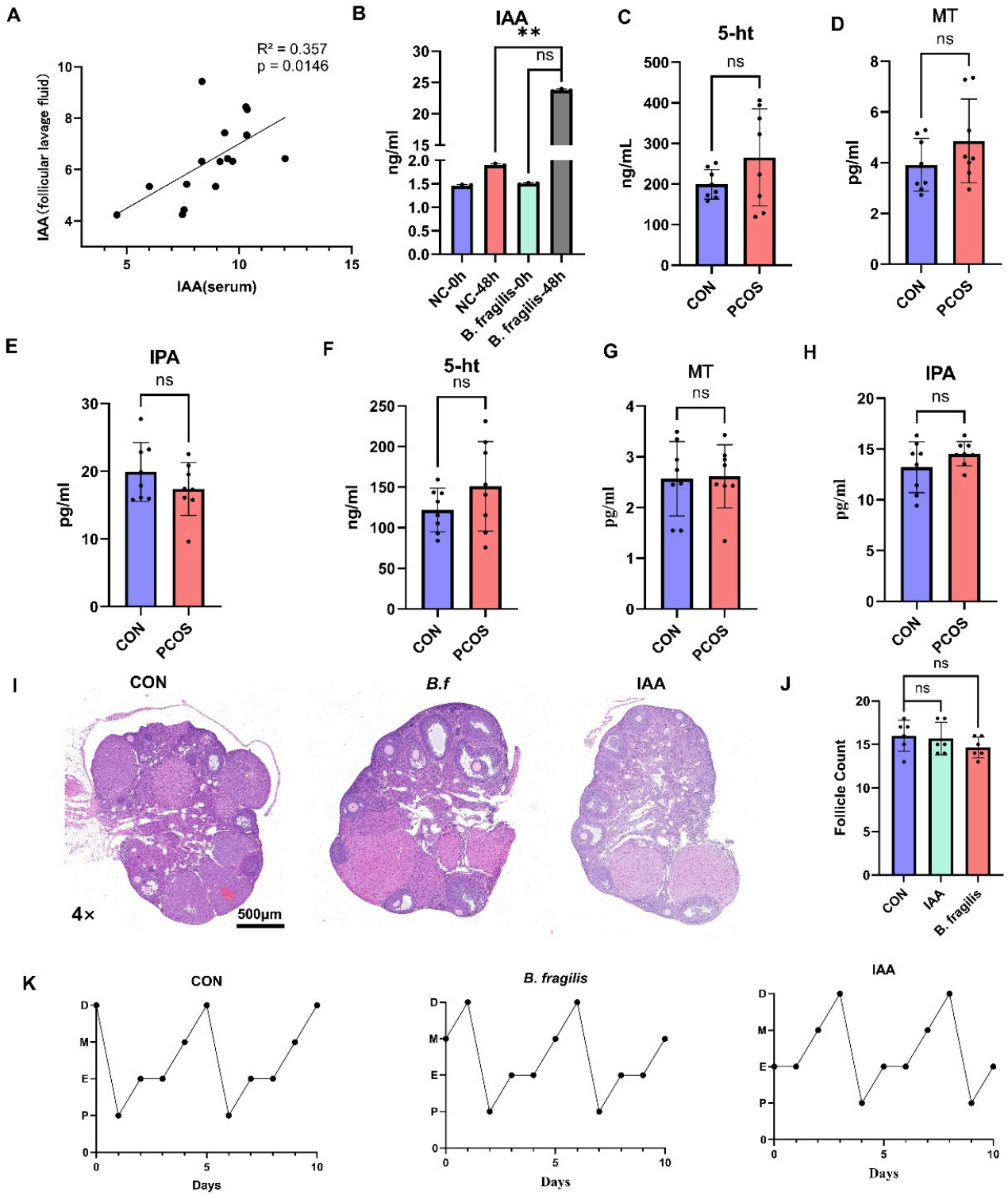


Figure 3

Functional assessment of the B. fragilis-IAA axis in PCOS

(A) Correlation analysis of IAA levels between serum and follicular fluid; (B) In vitro assessment of IAA production by *B. fragilis* under indole-supplemented conditions; (C–E) Levels of indole-3-propionic acid (IPA), 5-hydroxytryptamine (5-HT), and melatonin (MT) in serum; (F–H) Levels of IPA, 5-HT, and MT in follicular fluid; (I) Ovarian morphology assessed by H&E staining; (J) Quantification of follicle numbers; (K) Estrous cycle monitoring.

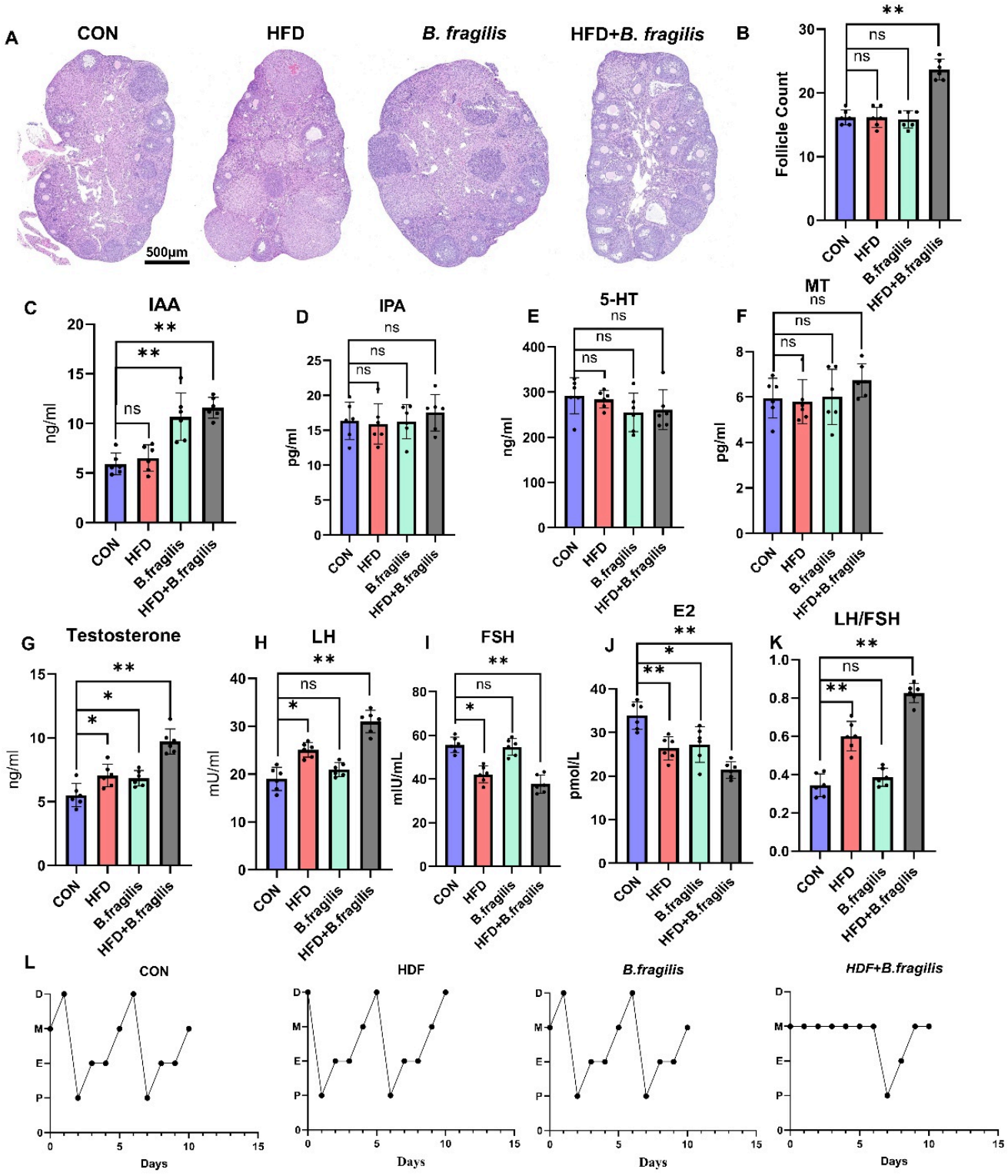


Figure 4

High-fat diet enables the pathogenic effect of B. fragilis in PCOS-like ovarian dysfunction

(A) Ovarian morphology assessed by H&E staining; (B) Quantification of follicle numbers; (C–F) Levels of indole-related metabolites, including indole-3-acetic acid (IAA), indole-3-propionic acid (IPA), 5-hydroxytryptamine (5-HT), and melatonin (MT); (G–K) Serum hormone levels, including testosterone, luteinizing hormone (LH), follicle-stimulating hormone (FSH), estradiol (E2), and the LH/FSH ratio; (L) Estrous cycle monitoring by vaginal smear analysis.

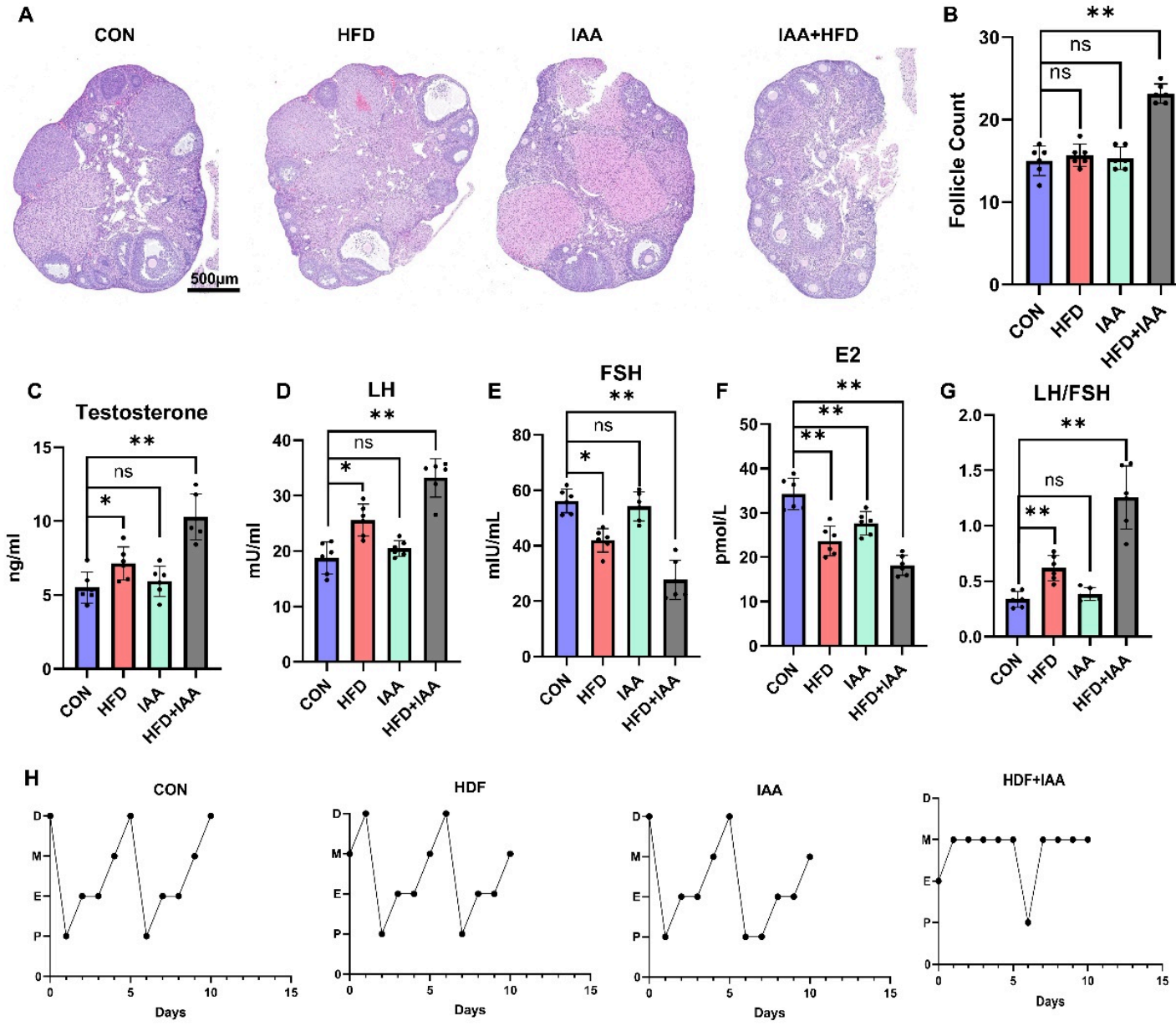


Figure 5

IAA mediates PCOS-like phenotypes under metabolic stress

(A) Ovarian morphology assessed by H&E staining; (B) Quantification of follicle numbers; (C–G) Serum hormone levels, including testosterone, luteinizing hormone (LH), follicle-stimulating hormone (FSH),

estradiol (E2), and the LH/FSH ratio; (H) Estrous cycle monitoring by vaginal smear analysis.

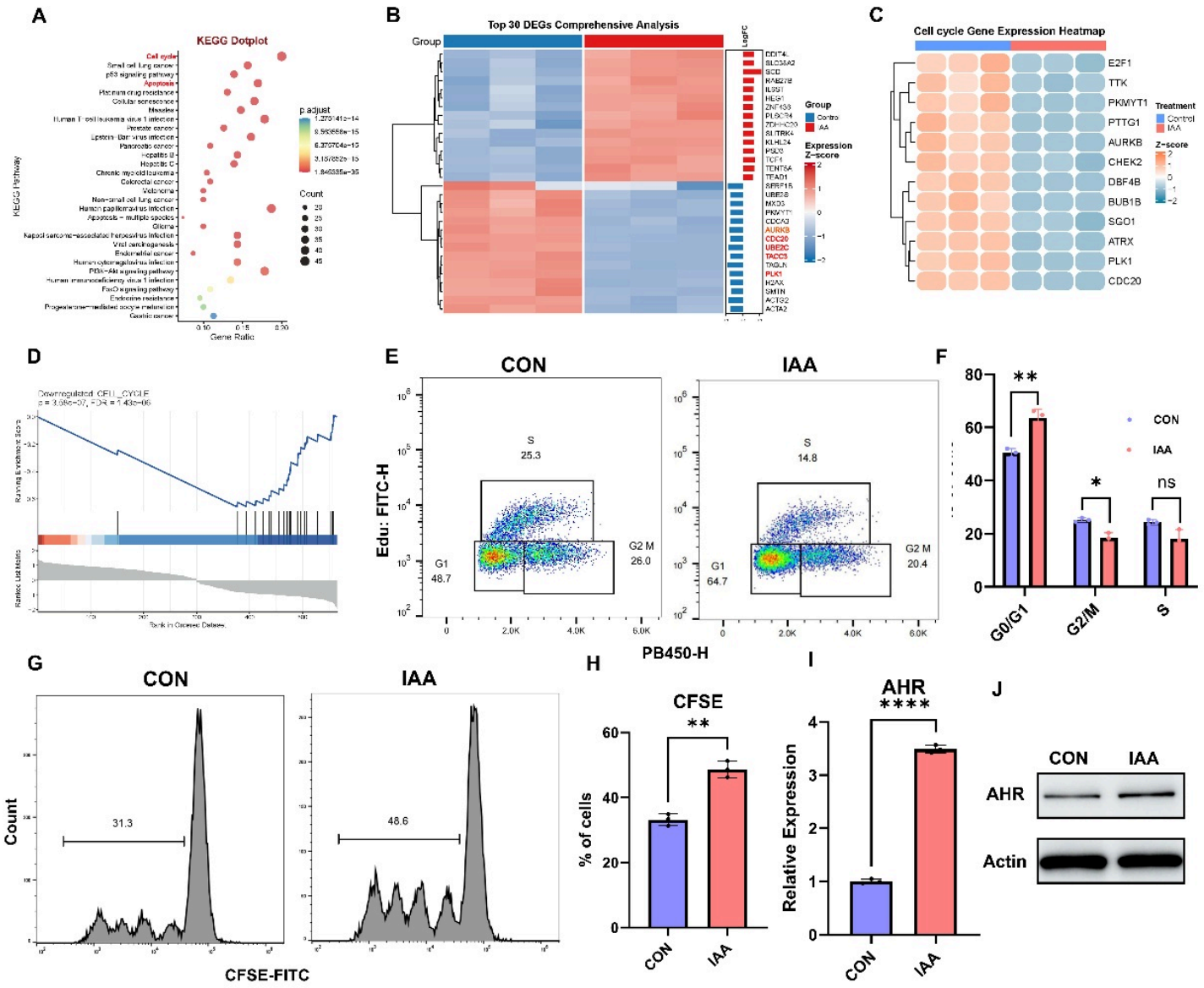


Figure 6

IAA impairs granulosa cell proliferation and activates AHR signaling

(A) Pathway enrichment analysis of RNA-seq data; (B) Top 30 differentially expressed genes; (C) Heatmap of cell cycle–related genes; (D) Gene set enrichment analysis (GSEA) of cell cycle–related pathways; (E) Flow cytometry analysis of cell cycle distribution; (F) Quantification of cell cycle phases; (G) CFSE assay of cell proliferation; (H) Quantification of proliferative capacity; (I) AHR mRNA expression assessed by qPCR; (J) AHR protein expression assessed by Western blot.

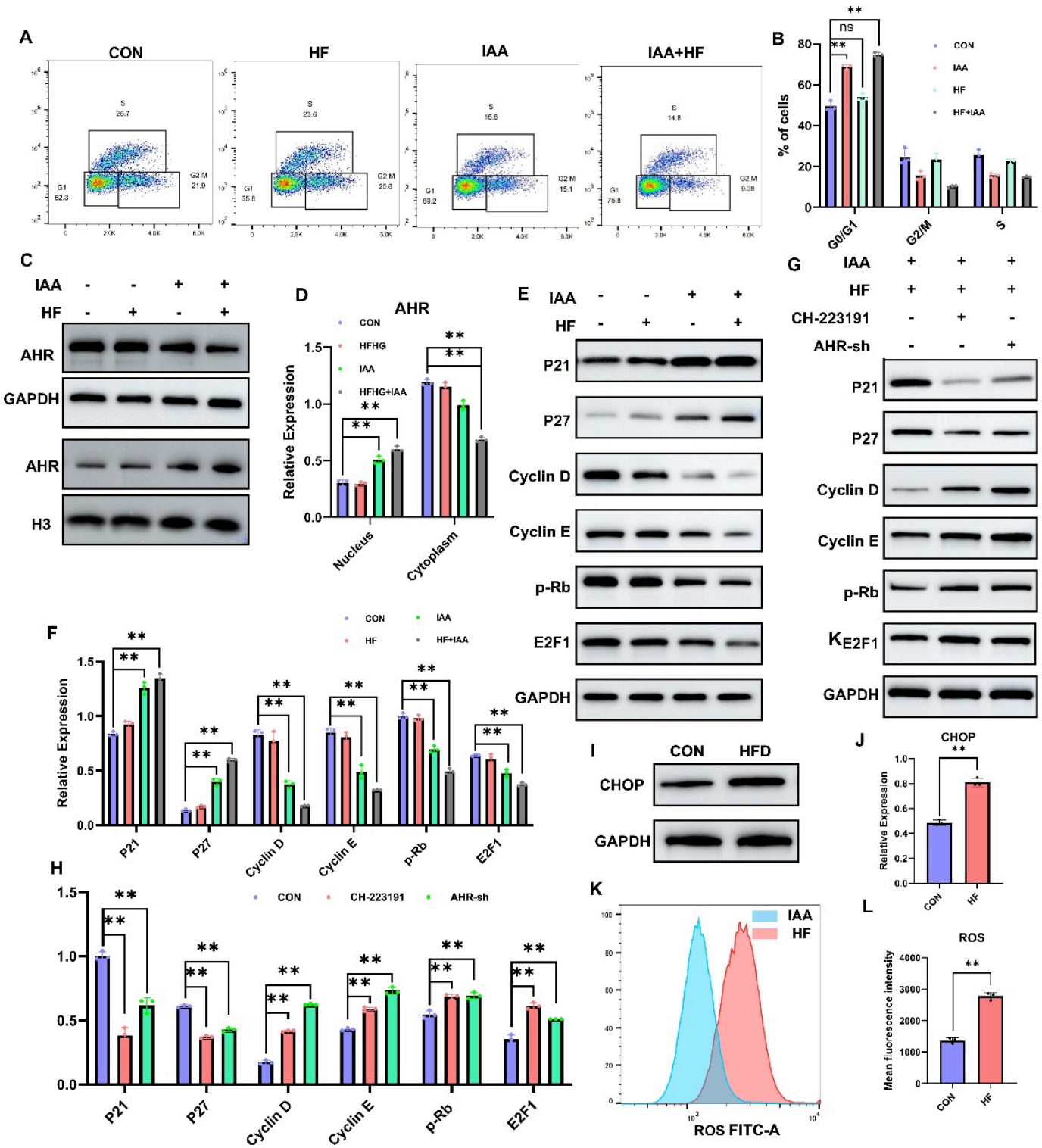


Figure 7

Lipotoxic stress potentiates IAA-induced AHR activation and cell-cycle arrest

(A) Flow cytometry analysis of cell cycle distribution following combined IAA and high-fat (HF) treatment; (B) Quantification of cell cycle phases; (C) AHR nuclear localization assessed by Western blot; (D) Quantification of nuclear AHR levels; (E) Expression of cell cycle–related proteins, including P21, P27,

Cyclin D, Cyclin E, phosphorylated Rb (p-Rb), and E2F1; (F) Quantification of protein expression levels; (G) Cell cycle analysis following AHR inhibition or knockdown; (H) Quantification of cell cycle distribution; (K) Intracellular ROS levels and CHOP expression under HF treatment.

Supplementary Files

This is a list of supplementary files associated with this preprint. Click to download.

- SupplementaryFile1UncroppedGelsandBlots.pdf
- FiguresS1S3.docx